Thermo-photo degradation of 2-propanol using a composite ceria-titania catalyst: Physico-chemical interpretation from a kinetic model

Mario J. Muñoz-Batista*, Ana M. Eslava-Castillo, Anna Kubacka, Marcos Fernández-García*

Instituto de Catálisis y Petroleoquímica, CSIC, C/ Marie Curie, 2, 28049 Madrid, Spain

ARTICLE INFO

ABSTRACT

This work describes a study carried out to construct and determine a kinetic formalism for the gas-phase degradation of 2-propanol using a combined thermo-photo based process. Outstanding catalytic performance was observed for a composite ceria-titania system with respect its parent ceria and titania reference systems. Thermo-photo as well as parallel photo- and thermal-alone experiments were carried out to interpret catalytic behavior. The kinetic experiments were conducted using a continuous flow reactor free of internal and external mass-heat transfer and designed using a Box-Behnken formalism. The kinetic expression developed for the thermo-photo degradation process explicitly includes the effect of the photon absorption in the reaction rate and leads to a mathematical formula with two components having different physico-chemical nature. This fact is used to settle down a fitting procedure using two steps (two separated experimental sets of data concerning temperature, light intensity, oxygen, water and/or 2-propanol concentrations) with, respectively, four and three parameters. The kinetic formalism was validated by fitting the experimental data from these two independent experiments, rendering a good agreement with the model predictions. The parameters coming from the kinetic modelling allow an interpretation of the catalytic properties of the ceria-titania catalyst, quantifying separately its enhanced performance (with respect to its parent systems) in the photonic and thermal components for the process. The procedure is applicable to a wide variety of thermo-photo processes in order to contribute to the understanding of their physical roots.

1. Introduction

Heterogeneous photocatalysis is considered to be one modern technology for decontamination of Volatile Organic Compounds (VOCs) [1]. One of most relevant advantages is that it operates under mild temperature and pressure conditions, and using oxygen from the air as the oxidizing agent [2–4]. As far as the materials are concerned, TiO_2 is the most used photocatalyst due to its good catalytic properties. It is also a relatively inexpensive and nontoxic material [2]. On the other hand, VOCs decontamination processes by photocatalysis show several disadvantages. Low quantum efficiency brought by recombination of photogenerated electrons and holes is usually reported [5–8]. In addition, titania appears only efficient for the removal of low concentration VOCs and displays low sunlight absorption due to its wide band gap (~3.2 eV for the anatase polymorph). For all these reasons it has a limited industrial application [2]. As a way to increase the profit from sunlight as well as to enhance quantum efficiency, surface sensitizers have been added to formulations based in titania. In particular the use of ceria has received significant attention. Ceria-titania (CeO_x-TiO_2)

composite materials have shown good photodegradation performance against a significant number of pollutants under different operation conditions, concerning gas or liquid phase, oxygen and water vapor concentration and other important variables in terms of catalytic output [9–25].

On the other hand, it is interesting to note that catalytic thermal oxidation has been actively used for VOCs elimination with satisfactory results. However, it is a high energy consuming technology and the search of good and stable catalysts appears as a key research activity in this field. Ceria is a common component in both classic and new formulations presenting promising catalytic activity [26–30].

Alternatively to both thermal or photon-based catalytic technologies, the combination of heat and light energy sources using the adequate catalytic material would drive to a convenient way to overcome most of the problems related to thermal or light alone based decontamination technologies. From a pure thermal perspective the reduction of the operation temperature with consequent lowering of the cost as well as reduction of catalyst deactivation processes can be mentioned [26–29]. From a photocatalytic perspective, the most important point

* Corresponding authors.
  E-mail addresses: jmunoz385x@gmail.com (M.J. Muñoz-Batista), mfg@icp.csic.es, m.fernandez@icp.csic.es (M. Fernández-García).

Nomenclature

A	Pre-exponential factor ($m^3\,mol^{-1}$)
a	Ratio external surface area per unit volume ($m^2\,m^{-3}$)
C	Molar concentration ($mol\,m^{-3}$)
E	Enhancement function (a.u.)
$e^{a,s}$	Local superficial rate of photon absorption (Einstein $cm^{-2}\,s^{-1}$)
Ea	Activation energy ($J\,mol^{-1}$)
F_A	Fraction of light absorbed (dimensionless)
F_R	Fraction of light reflected (dimensionless)
F_T	Fraction of light transmitted (dimensionless)
k	Kinetic constants (units depending on the reaction step)
N	Total number of data points
q_{sup}	Radiation flux on the catalytic film (Einstein $cm^{-2}\,s^{-1}$)
q_n	Net radiation flux (Einstein $cm^{-2}\,s^{-1}$)
R	Universal gas constant ($J\,mol^{-1}\,K^{-1}$)
RMSE	Root mean square error (%)
r	Superficial reaction rate ($mol\,m^{-2}\,s^{-1}$)
S	Surface concentration of sites for 2-propanol and water (Sites m^{-2})
S_1	Surface concentration of sites for oxygen (Sites m^{-2})
T	Temperature (°C)
v_z	Axial velocity ($m\,s^{-1}$)
x	Cartesian coordinate (m)
$\underline{x}$	Position vector (cm)
y	Cartesian coordinate (m)
z	Cartesian coordinate (m)
$[]_{ads}$	Adsorbed concentration on the catalytic surface ($mol\,m^{-2}$)
$\bar{\phi}$	Average primary quantum yield (mol of photons^{-1})

Subscripts

ads	Adsorption
exp	Experimental
g	Glass
in	Inlet
L_A	A lamp (See SI for details)
L_B	B lamp (See SI for details)
mod	Model
s	Sample
T	Thermo
$T - P$	Thermo-photo

Superscripts

↑	up direction (convention of signs, see SI for details)
↓	down direction (convention of signs, see SI for details)
*	Relative to thermo-photo-catalytic process

to overcome is the low reaction rates and consequently, low quantum efficiencies usually achieved [1–6]. Within this context, CeO_x-TiO_2 based and related materials would appear promising catalytic systems in thermo-photo catalysis. With photo-catalysis or thermo-catalysis and as above detailed, it has been proved that high activity can be achieved using CeO_x-TiO_2 based catalysts. Therefore, these materials recently launched the interest in composite systems and the synergetic effect between photo-catalysis and thermo-catalysis. Recent reports for cyclohexane and benzene degradation, $CO + O_2$ or $NO + CO$ reaction are some examples of thermo-photo-catalytic applications tested and showing activity enhancement with respect to thermal- and/or photo-only processes [31–38].

In this work, we describe a kinetic study concerning the temperature analysis of 2-propanol thermo-photo-degradation using TiO_2, CeO_2 and CeO_x-TiO_2 samples. 2-propanol is a volatile organic pollutant present at urban atmospheres and particularly at indoor environments. Among the most typical sources of this pollutant, we can enumerate construction materials, household products, waxes, varnishes and many others [39–41]. Therefore this pollutant appears a classical benchmark for gas-phase photo-oxidation processes. Using a kinetic approach we expect to contribute to the understanding of the physico-chemical basis of the 2-propanol thermo-photo-catalytic oxidation process. Although several works carried out studies concerning the performance CeO_x-TiO_2 catalysts, the understanding of the physical roots of such new decontamination process is still low. Moreover, none of the above mentioned works present a detailed kinetic study of the catalytic results [31–35]. To reach the primary objective of shed light into the thermo-photo-catalysis understanding, we developed a kinetic formulation containing an intrinsic (reaction rate) expression for the reaction occurring in a gas-phase thermo-photo-reactor employing thermal and UV light sources. The procedure solve the differential mass transfer equation, coupled with a nonlinear least-squares fitting algorithm to obtain kinetic parameter value estimations. Such kinetic study is based on the well-established initial steps of all thermo-photo-catalytic processes and included explicitly the radiation (light/thermal)-matter interaction. This allowed determining true kinetic constants providing general information, without any experimental bias concerning the experimental procedure and conditions used. The result of the study not only has

physico-chemical significance in terms of quantifying the different "thermo" and "photo" contributions to the reaction but also renders information required for scaling and design reactors [42–44].

2. Experimental section

2.1. Catalysts preparation

TiO_2, CeO_x and CeO_x-TiO_2 catalysts were prepared using a micro-emulsion preparation method. N-heptane (Scharlau) as organic media, Triton X- 100 (Aldrich) as surfactant and hexanol (Aldrich) as co-surfactant were used. Ultra pure water (Milli-Q) was used as aqueous phase [45]. The TiO_2 sample was obtained in a microemulson using titanium tetraiso-propoxide as precursor. This precursor was introduced into the microemulsion drop by drop from a solution with isopropanol (2:3 v/v) [46]. CeO_2-TiO_2, and CeO_2 samples were obtained from cerium nitrate (Alfa Aesar) precursor using a stoichiometric quantity of tetramethylammonium-hydroxide (TMAH) to obtain 2.5% of Ce(III) hydroxide. Then, titanium tetraisopropoxide was introduced into the previously resulting microemulsion. Water/(Ti, Ce or Ti + Ce) and water/surfactant molar ratios were, 110 and 18 for all samples [46,47]. The resulting mixture was stirred for 24 h and centrifuged to separate the solid. The separated solid precursors were rinsed with methanol and dried at 110 °C for 12 h. After drying, the solid precursors were subjected to a heating ramp (rate 1 °C min^{-1}) up to 500 °C, maintaining this temperature for 2 h.

2.2. Catalysts characterization

UV–vis diffuse-reflectance spectroscopy experiments using $BaSO_4$ as a reference were performed with a Shimadzu UV2100 apparatus. The surface areas (Brunauer–Emmett–Teller (BET)), average pore volumes and sizes were measured by nitrogen physisorption (Micromeritics ASAP 2010). XRD profiles were obtained with a Seifert D-500 diffractometer using Ni-filtered Cu Kα radiation. XPS data were recorded on $4 \times 4\,mm^2$ pellets, 0.5 mm thick. The SPECS spectrometer main chamber, working at a pressure $< 10-9$ Torr, was equipped with a PHOIBOS 150 multichannel hemispherical electron analyzer with a

dual X-ray source working with Ag Kα (hν = 1486.2 eV) at 120 W, 20 mA using C 1s as energy reference (284.6 eV). Optical properties of the catalytic film (Transmittance and Reflectance) were measured with the Shimadzu UV2100 apparatus using 1×1 cm^2 pyrex glass and ca. 0.4 mg cm^{-2}.

2.3. Thermo-photo catalytic activity

The thermo-photo activity of the samples for 2-propanol oxidation was tested using a continuous flow annular thermo-photo-reactor (pyrex) schematically depicted in Fig. 1. The catalyst (ca. 0.4 mg cm^{-2}) was deposited onto the inner tube as a thin layer from a suspension in ethanol. During thermo- and thermo-photo-catalytic tests, the film was heated using a cartridge heater. The temperature of the layer was controlled and monitored by a temperature controller (Toho TTM-005) and K-type thermocouple inserted into the reactor. Minimal (below 1 °C) axial temperature variation was reached with a cartridge heater (230 V; 500 W; "Resistencias RSI INCOLOID800") having controlled/compensated homogeneous heating. The UV irradiation was generated by four fluorescent UV lamps (Philips TL 6 W/08-F6T5 BLB, 6 W) symmetrically positioned outside the reactor. The reacting mixture (100 mL min^{-1} and 20 vol% O$_2$/N$_2$) was prepared from pure N$_2$ and O$_2$. The 2-propanol concentration was varied from 1200 to 2400 ppm by vaporization of organic compound. N$_2$ was used to transport the gas-phase products from the liquid-containing saturators to the mainstream and distilled water was injected using a syringe pump. The irradiation level on the catalytic film was modified by means of neutral optical filters. The catalytic properties were evaluated at 3 h from the start of the irradiation, where a pseudo-stationary situation is reached. The concentrations of the reactant was analyzed using an online gas chromatograph (Agilent GC 6890) equipped with HP-PLOT-Q/HP-Innowax columns (0.5/0.32 mm I.D. ×30 m) and thermal conductivity and flame ionization detectors.

3. Results and discussion

3.1. Characterization summary

Although this work focuses on the kinetic analysis of the thermo-photo-degradation of gas phase 2-propanol, it includes a brief section concerning the characterization details of the samples. XRD (X-ray diffraction), UV–vis (UV–vis spectroscopy), microscopy, and XPS (X-ray photoelectron spectroscopy) experimental results are present in the Supporting Information document ("characterization results" section;

Figs. S1–S3; Table S1). Table 1 shows a summary of chemical, morphological and optical properties of the three samples under study. Such table shows good correspondence between theoretical and real (measured) molar% of samples obtained with TXRF (Total Reflection X-ray Fluorescence). The table also presents the percentage of Ce at the surface of the anatase dominant phase for the CeTi composite sample and obtained by XPS. The table shows the similitude of the materials in terms of surface area (95–102 m^2 g^{-1}), porosity properties and crystal size of the anatase phase (JCPDS card 78–2486, corresponding to the I41/and space group), around 10 nm for the Ti and the CeTi composite samples. The microscopy analysis (Fig. S2) provides additional evidence of the similar morphology of the Ti and CeTi samples. The pure fluorite ceria sample (JCPDS card 87-0792, corresponding to the Fm3m space group) showed a crystallyte size of 8.5 nm. The combined use of all the above mentioned techniques (particularly XRD and Electron Diffraction) indicates that ceria is at surface of the anatase component, without detection of any doping effect of the anatase structure. The last column of Table 1 presents the band gap of the samples assuming an indirect gap semiconductor for all cases. The results display typical values for pure TiO$_2$ and CeO$_2$, and a 2.97 eV value for the composite CeTi sample. [47,48]

3.2. Kinetic modelling formalism

According to the reactor geometry presented in Fig. 1 and under kinetic control regime (See "external and internal mass-heat transfer" analysis in the Supporting Information section), differential mass balance equation for 2-propanol oxidation can be expressed as:

$$v_z \left(\frac{dC_{C_3H_8O}}{dz} \right) = a\, r_{C_3H_8O} \tag{1}$$

Where v_z, a, $C_{C_3H_8O}$ and $r_{C_3H_8O}$ are, respectively; the axial velocity, the external catalytic surface area per unit volume, the 2-propanol concentration and the average reaction rate. To solve Eq. (1), one boundary condition is necessary:

$$C_{C_3H_8O}(z=0) = C_{C_3H_8O,in} \tag{2}$$

In Eq. (2), $C_{C_3H_8O,in}$ denote 2-propanol inlet concentration.

Eq. (2) takes into consideration only the convective flow through axial coordinate z, which is a typical approach for this configuration reactor [49–52]. Besides, the following assumptions were considered: (i) the reactor operates under steady state conditions, (ii) negligible axial diffusion when compared to the convective flux in that direction, and (iii) negligible homogeneous (photo or thermo) chemical reactions.
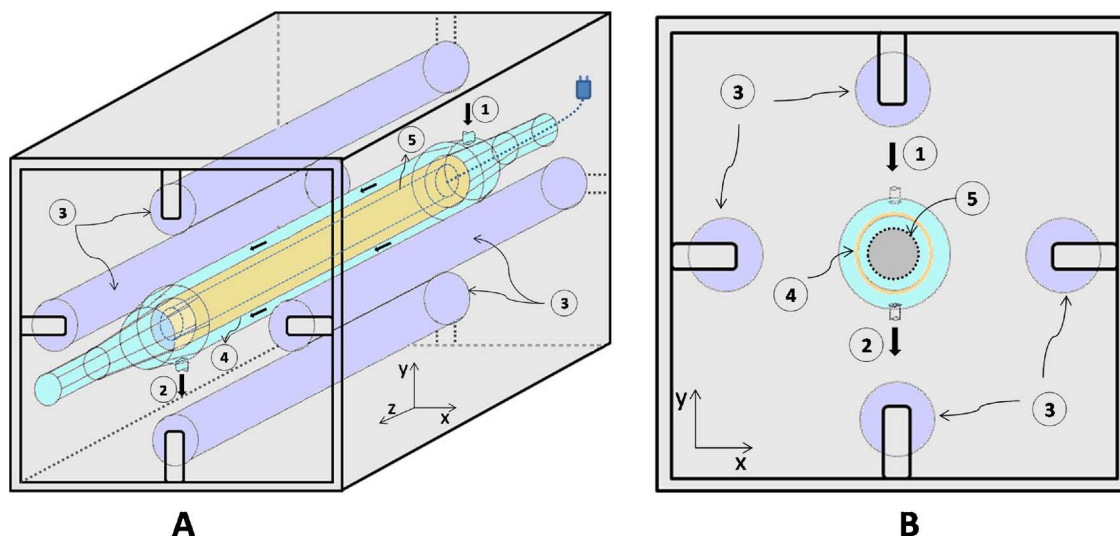

Fig. 1. (A) Thermo-photo-catalytic annular reactor. (B) Side section view. (1) Gas inlet, (2) gas outlet, (3) UV lamp, (4) catalyst sample, (5) cartridge heater.

Table 1
Optical, structural and morphological properties of the samples.[a]

sample	TXRF/XPS	XRD		N₂ physisorption			UV–vis
	Ce/Ti atomic ratio	Size (nm)[b]	Cell parameters (Å)[c]	BET surface area (m² g⁻¹)	pore volume (cm³ g⁻¹)	pore size (nm)	Band gap (eV)
Ti	–	12.1	3.789/9.481	95.8	0.123	5.2	3.20
CeTi	0.03/0.10	13.7	3.794/9.497	97.2	0.112	4.2	2.97
Ce	–	8.5	5.403	101.2	0.120	5.0	2.55

[a] Standard error: band gap 0.04 eV, BET 1.5 m g⁻¹; pore parameter 8%, size 0.5 nm, cell parameters 0.003 A, Ce/Ti ratio, 0.02.

[b] For anatase TiO_2 in the case of the Ti and CeTi samples and CeO_2 for Ce.

[c] a = b/c for anatase TiO_2 and a for CeO_2.

More details about the mass balance equation deduction are presented in the Supporting Information (section "mass balance").

In order to solve Eq. (1), a formalism concerning the reaction rate was obtained based on the reaction scheme summarized in Table 2. This simplified scheme considers the well-established initial steps of the thermo-photo-catalytic processes. Under UV irradiation, the photo-excited sample generates electrons and holes. The holes predominantly react with adsorbed water and superficial OH anions producing OH· radicals. On the other hand, electrons may react with adsorbed oxygen to generate $O_2^{°-}$ radicals [49,53–55]. Recombination process between electrons and holes in the bulk or surface of the particles are also usually reported [49,53–56]. Two parallel pathways (step 4 of Table 2) have been considered in this work for 2-propanol degradation. Photo-related degradation of the organic molecule is mostly carried using holes while thermal-related degradation requires oxygen, as broadly admitted in the literature. [1–6,57–61] Using the reaction scheme discussed, the degradation rate can be expressed as Eq. (3).

$$r_{C_3H_8O_{T-P}} = -(k_{4.1}[C_3H_8O]_{ads}[OH^°] + k_{4,2}[C_3H_8O]_{ads}[O_2]_{ads}) \quad (3)$$

As it is described in detail in Section "kinetic equation" of the Supporting Information and using typical approximations for this kind of reactions, the equation rate for thermo-photo-catalytic oxidation of 2-propanol is defined by Eq. (4).

Table 2
Simplified reaction scheme for the thermo-photo catalytic degradation of 2-propanol.

Step	Kinetic equation	rate
0	$Cat + \xrightarrow{h\nu} Cat + h^+ + e^-$	rg
1	$h^+ + H_2O_{ads} \rightarrow OH^° + H^+$	$k_1[H_2O]_{ads}[h^+]$
	$h^+ + OH^-_{ads} \rightarrow OH^°$	
2	$e^- + O_{2\,ads} \rightarrow O_2^{°-}$	$k_2[O_2]_{ads}[e^-]$
3	$h^+ + e^- \rightarrow heat$	$k_3[h^+][e^-]$
4	$C_3H_8O_{ads} + OH^° \rightarrow Products$	$k_{4.1}[C_3H_8O]_{ads}[OH^°]$
	$C_3H_8O_{ads} + O_2 \xrightarrow{T} Products$	$k_{4.2}[C_3H_8O]_{ads}[O_2]_{ads}$
5	$OH^° + M \rightarrow Products$	$k_5[OH^°]_{ads}[M]$

temperature and universal gas constant, respectively. Note that we use the notation without asterisk for the thermo-catalytic process while A_i^* and Ea_i^* are used exclusively for the photo- and thermo-photo-catalytic processes.

The reaction was examined under several levels of 2-propanol initial concentration, temperature, water concentration and irradiation levels. Near null dependence of the reaction rate with respect to the O₂ concentration was identified in thermo-catalytic tests while a linear dependence was detected for 2-propanol in thermo-catalytic and thermo-

$$r_{C_3H_8O_{T-P}} = -\left(\frac{k\exp-\frac{(Ea_{C_3H_8O}^* + Ea_{H_2O}^*)}{RT}C_{C_3H_8O}C_{H_2O}\sqrt{e^{a,s}}}{\left(1 + A_{C_3H_8O}^*\exp-\frac{Ea_{C_3H_8O}^*}{RT} + A_{H_2O}^*\exp-\frac{Ea_{H_2O}^*}{RT}C_{H_2O}\right)} \times \frac{1}{\left(1 + A_{C_3H_8O}^*\exp-\frac{Ea_{C_3H_8O}^*}{RT}C_{C_3H_8O} + A_{H_2O}^*\exp-\frac{Ea_{H_2O}^*}{RT}C_{H_2O} + k'\exp-\frac{Ea_{C_3H_8O}^*}{RT}C_{C_3H_8O}\right)}\right.$$
$$\left. + \frac{k''\exp-\frac{(Ea_{C_3H_8O} + Ea_{O_2})}{RT}C_{C_3H_8O}C_{O_2}}{\left(1 + A_{C_3H_8O}\exp-\frac{Ea_{C_3H_8O}}{RT}C_{C_3H_8O} + A_{H_2O}\exp-\frac{Ea_{H_2O}}{RT}C_{H_2O}\right)\left(1 + A_{O_2}\exp-\frac{Ea_{O_2}}{RT}C_{O_2}\right)}\right) \quad (4)$$

Where k, k' and k'' kinetic constants are given by:

$$k = \frac{k_{4.1}[S]^2 k_1 A_{C_3H_8O}^* A_{H_2O}^*}{\gamma}\sqrt{\frac{\overline{\phi}}{k_3}} \quad (5)$$

$$k' = \frac{k_{4.1}[S]\,A_{C_3H_8O}^*}{\gamma} \quad (6)$$

$$k'' = k_{4.2}[S][S_1]A_{C_3H_8O}A_{O_2} \quad (7)$$

The first summand defines the 2-propanol elimination due to photo and thermo-photo processes while the second one concerns exclusively the pure thermo-catalytic process. As it is thoroughly described in the supplementary information section, for both, thermo-photo- and pure thermo- adsorption processes, the Arrhenius equation (expressed in its general form as Eq. (8)) was used.

$$k_i = A_i \exp\frac{-Ea_i}{RT} \quad (8)$$

Where i runs over all reactants of the reaction (C_3H_8O, H_2O, and O_2), A is pre-exponential factor, Ea is the activation energy, and T and R are

photo-catalytic tests. The corresponding experimental evidences are presented in Figs. S8 and S9 of the supporting information section. This behavior suggests that the kinetic expression can be simplified to Eq. (9). We note that the approximation methodology just described has been previously used by other authors in the study of photo-catalytic processes [53,55].

$$r_{C_3H_8O_{T-P}} = -\left(\frac{k\exp-\frac{Ea^*}{RT}C_{C_3H_8O}C_{H_2O}\sqrt{e^{a,s}}}{\left(1 + A_{H_2O}^*\exp-\frac{Ea_{H_2O}^*}{RT}C_{H_2O}\right)}\right.$$
$$\left. + \frac{k'\exp-\frac{(Ea)}{RT}C_{C_3H_8O}}{\left(1 + A_{H_2O}\exp-\frac{Ea_{H_2O}}{RT}C_{H_2O}\right)}\right) \quad (9)$$

In this Equation the activation energy of 2-propanol and water or oxygen were grouped into the Ea^* (thermo-photo-) and Ea (thermo-) constants as follows:

$$Ea^* = Ea_{C_3H_8O}^* + Ea_{H_2O}^* \quad (10)$$

$$Ea = Ea_{C_3H_8O} + Ea_{O_2} \tag{11}$$

The "isolated" thermo kinetic modelling of 2-propanol degradation was solved in a first step of the procedure. The experimental measurements carried out in the case of the thermo-catalytic process are collected in Table S2 of the Supporting Information. The goal of the corresponding experiments was to obtain the kinetic information under thermal (dark) reaction conditions. For this, the influence of 2-propanol initial concentration, water concentration and temperature (3 levels for each factor and Box–Behnken design) were analyzed using Eq. (12), with k'' defined by Eq. (13).

$$r_{C_3H_8O_T} = -\frac{k'' \exp-\frac{(Ea)}{RT}C_{C_3H_8O}}{\left(1 + A_{H_2O} \exp-\frac{Ea_{H_2O}}{RT}C_{H_2O}\right)} \tag{12}$$

$$k'' = k_{4.2}[S][S_1]A_{C_3H_8O}A_{O_2}C_{O_2} \tag{13}$$

To this end, a MATLAB® R2010b algorithm was build-up to obtain the kinetic parameters using a subroutine to solve the differential Eq. (1) (subroutine ode45 based in a Runge-Kutta formalism) subjected to boundary condition (Eq. (2)), coupled with a nonlinear least-squares fitting algorithm (lsqnonlin, Algorithm: Trust-Region-Reflective Optimization) to obtain the parameters of Eq. (12). The analysis of errors in the kinetic parameters was carried out using the MatLab "nlparci" subroutine. The "nlparci" subroutine returns the 95% confidence intervals for the nonlinear least squares parameter estimates using the Jacobian matrix associated to Eq. (12) as well as the experimentally measured errors obtained for the reaction rate. Once the corresponding parameters of Eqs. (11)–(13) were obtained, this information, uncoupled to the thermo-photo-process, can be used as known parameters in Eq. (9).

Before solving the thermo-photo-catalytic kinetic model (Eq. (9)), the local superficial rate of photon absorption ($e^{a,s}$) was determined. This observable can be defined by Eq. (14).

$$e^{a,s}(\underline{x}) = q_{sup}(\underline{x})F_{As} \tag{14}$$

Where F_{As} is the fraction of light absorbed by the sample and q_{sup} the radiation flux at each position (x,y,z) of the catalytic film (see details in Supporting information; "radiation model" section). This radiation flux can be obtained using Eq. (15).

$$q_{sup} = \sqrt{{}^xq2 + {}^yq2} \tag{15}$$

Where

$${}^xq = {}_{L_A}^{x}q_1^{\uparrow} + {}_{L_B}^{x}q_1^{\uparrow} + {}_{L_A}^{x}q_2^{\downarrow} + {}_{L_B}^{x}q_2^{\downarrow} \tag{16}$$

$${}^yq = {}_{L_A}^{y}q_1^{+} + {}_{L_B}^{y}q_1^{+} + {}_{L_A}^{y}q_2^{-} + {}_{L_B}^{y}q_2^{-} \tag{17}$$

$${}_{L_A}^{x}q_1^{\uparrow}, {}_{L_B}^{x}q_1^{\uparrow}, {}_{L_A}^{x}q_2^{\downarrow}, {}_{L_B}^{x}q_2^{\downarrow}, {}_{L_A}^{y}q_1^{+}, {}_{L_B}^{y}q_1^{+}, {}_{L_A}^{y}q_2^{-}, {}_{L_B}^{y}q_2^{-} = f\left(q_n, F_{T_s}, F_{T_g}, F_{R_s}, F_{R_g}\right) \tag{18}$$

The Supporting information file shows the details of the model procedure followed to obtain q_{sup}. The model requires the representation of a three-dimensional light source. It assumes superficial emission model for the lamps and use the ray-tracing method considering all optical events occurring on the reaction system (light-reactor-matter). The model provides a formulation to describe q_{sup} at each point of the catalytic surface as a function of q_n (local net radiation flux) as well as the light fractions transmitted and reflected (F_T and F_R) at each component (sample, s, or glass, g) of the reactor (Fig. 2). Fig. 2 shows also the UV lamp spectral distribution.

Fig. 3 presents the local superficial rate of photon absorption profiles expressed in Cartesian coordinates, for Ti and CeTi samples. The rise in absorption capacity for the sample with cerium was evident and in agreement with the Band Gap modification presented in Table 1. Besides, no particular geometrical differences were detected. Average values of 1.0×10^{-8} and 1.1×10^{-8} Einstein $cm^{-2} s^{-1}$ (100%

Irradiation level), for Ti and CeTi were obtained. This average value can be used in Eq. (9) for the kinetic analysis.

Finally, the thermo-photo kinetic model was solved (Eqs. (1) and (9) and the same MATLAB algorithm described before) using the experimental data summarized in Table S3. Table S3 data corresponds, as mentioned previously, to experimental conditions selected according to Box–Behnken design of four factors and three levels.

3.3. Experimental study of the activity; application of the kinetic modelling

The rate of 2-propanol oxidation measured for the photo-, thermo- and photo-thermo-processes is presented in Fig. 4 for the three samples. Photo-catalytic experiments are run at room temperature while the other two experiments are carried out in the 220–270 °C, tanking data each 10 °C. The selectivity output of the 2-propanol oxidation in representative operating conditions is summarized in Table S4. As can be seen in Fig. 4, Ti and CeTi samples show significantly higher activity than the Ce material under illumination. This is a well-known fact [1–6]. The materials start to present activity under heat at 220 °C. The growth of the reaction rate is noticeable for all samples but specially in those containing titania. Higher rates are observed under the combined use of light and heat if compared with both photo and thermal processes. This is somehow a general observation for all samples under study although the difference between pure thermo and thermo-photo processes is rather small for the Ce samples. To analyze this point, in Fig. 5 we plot what we call the enhancement function (E), measured as:

$$E = \text{rate (Thermo-photo)} - (\text{rate (Photo)} + \text{rate (Thermo)}) \tag{19}$$

Fig. 5 indicates that the enhancement factor is essentially inexistent in Ce. For Ti, it shows a marked temperature dependence, being only positive (and thus favorable with respect to an additive combination of thermo- and photo-based processes) for high temperature. For CeTi we observe a range of temperatures where the thermo-photo process is neatly favorable and has clear advantages with respect to the reference systems. This observation opens the opportunity of using ceria-titania composite systems as an interesting base material for thermo-photo catalytic processes.

As mentioned, to interpret the outstanding properties of the CeTi material in the thermo-photo-degradation of 2-propanol, we carried a complete kinetic study of the catalytic behavior. The kinetic analysis renders the parameter values presented in Table 3. Model prediction is a result of a complex calculation outlined in the previous subsection 2.2. It should be here recalled that Eqs. (1) and (9) were used as the kinetic expression, valid for the experimental working conditions. The quality of the model fit was evaluated with the root mean square error (RMSE) between the experimental (exp) value and the modelling (mod)
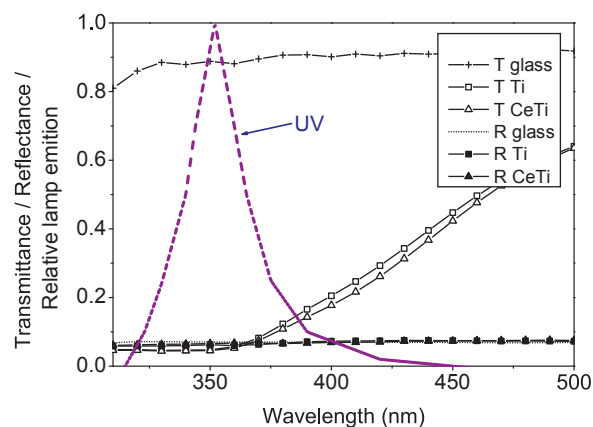

Fig. 2. Transmittance and Reflectance of the Ti and CeTi samples and spectral distribution of the Lamp.
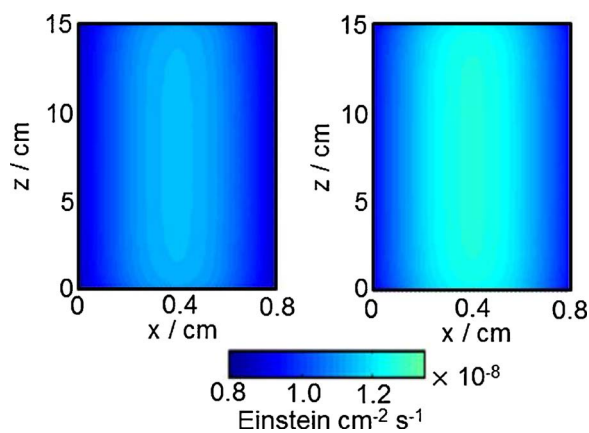
Fig. 3. Local superficial rate of photon absorption for TiO₂ (First panel) and CeOₓ-TiO₂ (Second panel) samples.

described by Eqs. (1) and (9). In Eq. (20) N is the total number of data points.

$$\text{RMSE} = \sqrt{\frac{1}{N}\sum_{1}^{N}\left(\frac{C_{C_3H_8O_{(exp)}} - C_{C_3H_8O_{(mod)}}}{C_{C_3H_8O_{(exp)}}}\right)^2} \times 100 \tag{20}$$

Note that our calculation consider a full analysis of the error including both the standard error observed in the 2-propanol

concentration or disappearance rate as well as the one related to the fitting procedure based in the minimization of the square of the differences between the model and the experiment. A good fitting with 5.1 and 6.5 of root mean square error was obtained for Ti and CeTi samples, respectively. The goodness of the fitting is also evident in Fig. 6, in which the comparison of the outlet 2-propanol experimental and simulated concentration for the CeTi sample shows a neat, good correlation. In brief, the small RMSE validates the goodness of our model and approach.

In order to interpret the physical basis of the CeTi performance we display in Fig. 7 the ratio of the kinetic parameters obtained for this sample and the Ti reference. The Ti reference is the reference having high photo-catalytic activity and some interest in thermo-photo-catalytic processes. Thus we particularly emphasize the factors which will drive the significant thermo-photo activity of the CeTi sample with respect to the well-known Ti reference. Titania is, on the other hand, the dominant component of the CeTi sample. Nevertheless, we note that using the Ce sample as reference seems relatively of low interest as this system has essentially no thermo-photo activity. The thermal activity seems to command the Ce behavior as a function of the temperature presented in Figs. 4 and 5.

From Fig. 7 we first observe that activation energy and pre-exponential factors corresponding to adsorption processes are essentially similar in the two catalysts, CeTi and Ti. As the Ce content of Ti is relatively minor (as already mentioned) this may sound reasonable. Importantly, the results indicate that the adsorption of water and 2-
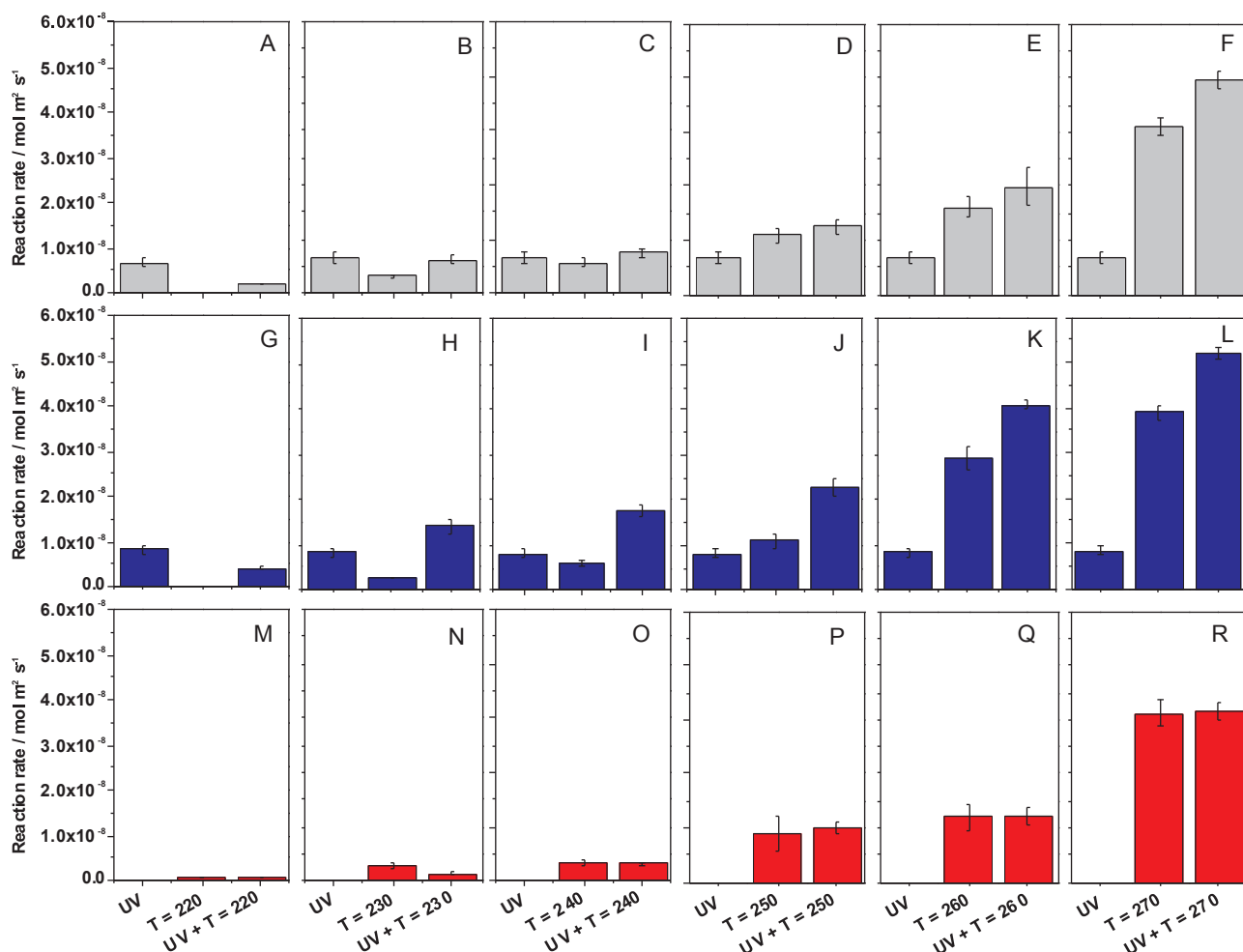

Fig. 4. Temperature influence in thermo- and photo-thermo-catalytic oxidation of 2-propanol. TiO₂ (gray), CeTi (blue) and CeO₂ (red). Experiment under UV illumination are carried out at RT. Thermal (described by a T) or Thermo-photo- (described as UV + T) runs are carried out in the 220–270 °C interval. (For interpretation of the references to colour in this figure legend, the reader is referred to the web version of this article.)
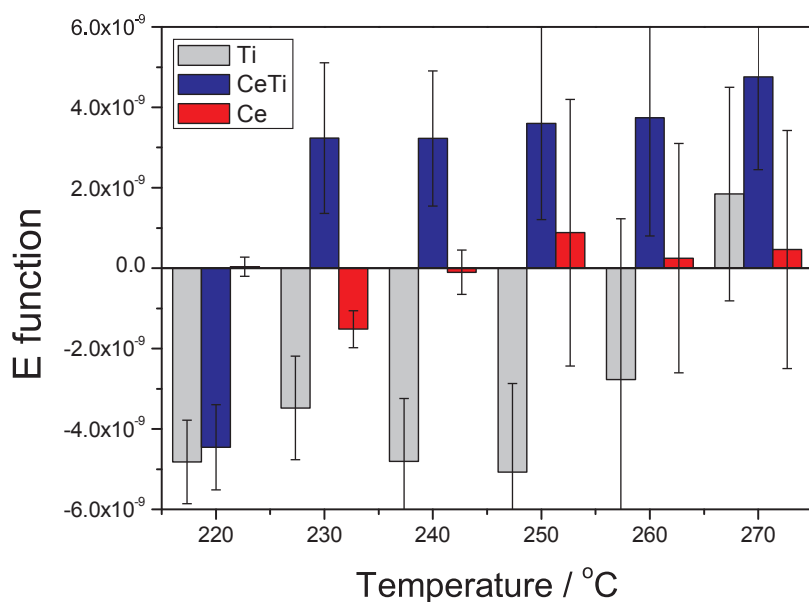
propanol are essentially equal in the two materials. This help in the interpretation of the k and k'' behavior. According to Eqs. (5) and (13) and assuming no change in the surface adsorption sites, we can observe that:

$$\text{ratio}(k) = \frac{(k_{4.1}k_1)_{\text{CeTi}}}{(k_{4.1}k_1)_{\text{Ti}}} \frac{\left(\sqrt{\frac{\bar{\phi}}{k_3}}\right)_{\text{CeTi}}}{\left(\sqrt{\frac{\bar{\phi}}{k_3}}\right)_{\text{Ti}}} \tag{21}$$

$$\text{ratio}(k'') = \frac{(k_{4.2})_{\text{CeTi}}}{(k_{4.2})_{\text{Ti}}} \tag{22}$$

We previously measured the ratio between the $\left(k_1\sqrt{\frac{\bar{\phi}}{k_3}}\right)$ factor for CeTi and Ti samples and this has a value of 1.21 [47]. Considering this value and using Eqs. (21) and (22), we can infer that the CeTi sample has an enhanced response (with respect to the Ti sample) in the $k_{4.1}$ and $k_{4.2}$ kinetic constants. Such enhancement ratio has 1.33 and 1.32 values for, respectively, $k_{4.1}$ and $k_{4.2}$. Taking into account these three factors we can conclude that the CeTi has photo, thermo, and thermo-photo capabilities improved with respect to the Ti (and Ce) references by a number of physico-chemical factors.

In first place, CeTi presents an enhanced ratio between step one of the kinetic model (the creation of hole-related radicals) and step three, which accounts for the annihilation of radicals (Table 2). Thus the $\left(k_1\sqrt{\frac{\bar{\phi}}{k_3}}\right)$ factor renders information about the availability of radical species during reaction. CeTi is a better photocatalyst than the parent Ti
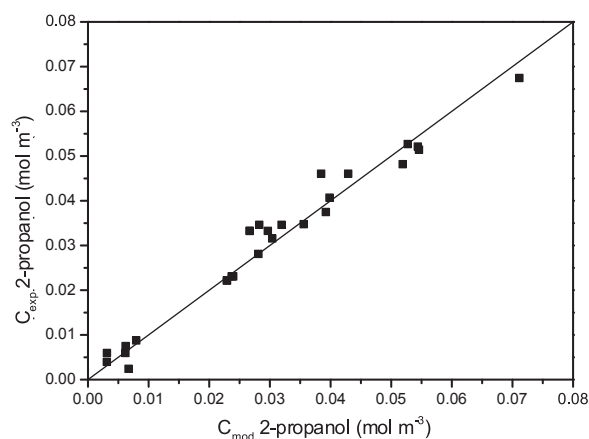

Fig. 6. Parity plot of experimental data against predicted data given by kinetic model.

and this is ascribed to a better handling of charge carrier with direct implications in decreasing the recombination of charge. The photoluminescence study presented in Fig. S3 demonstrates this point by comparing the overall intensity observed for a physical mixture of the Ce and Ti samples and the CeTi sample. The lower intensity of the CeTi sample is obvious form the plot. As well known, this is a consequence of the decrease in charge recombination and is directly reflected in a positive influence in photoactivity for the CeTi sample [49]. Secondly, the CeTi appears to improve (with respect to the Ti reference) the

Table 3
Kinetic Parameters for CeTi and Ti samples.

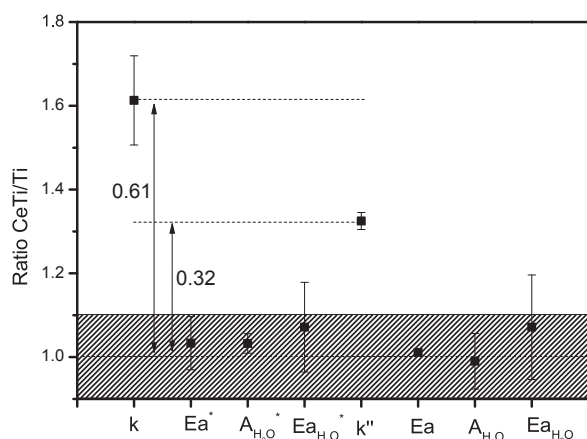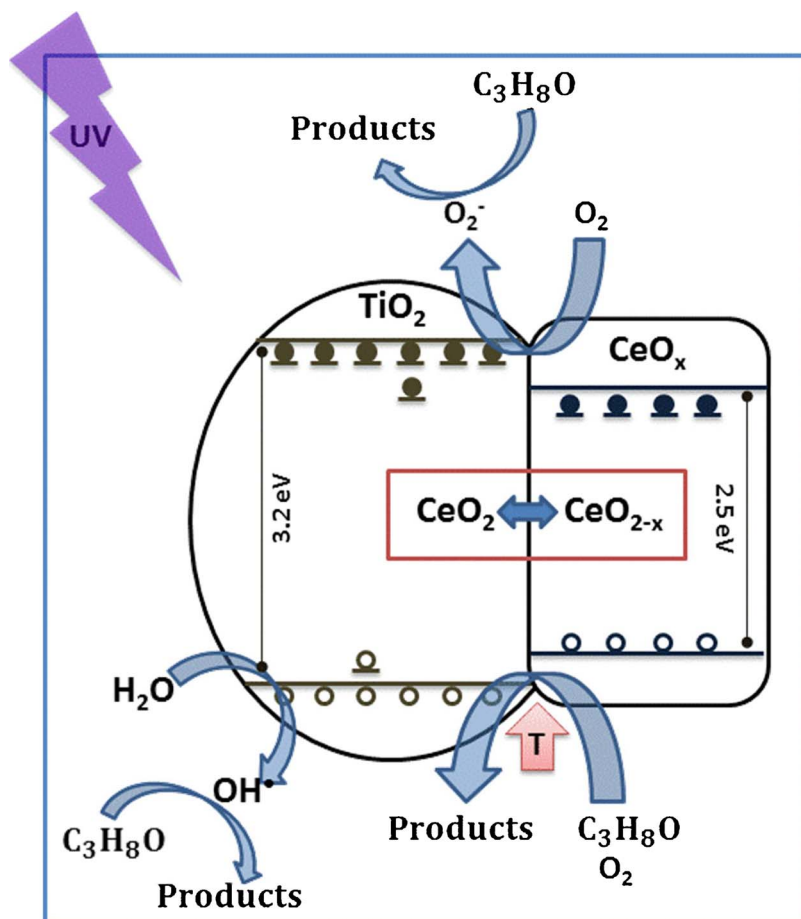| Constant	Value		Units	Error	
	Ti	CeTi		Ti	CeTi
k	3.1×10^{11}	5.0×10^{11}	$(\text{m}^3_{\text{mix}})^2 \, \text{m}^{-1}_{\text{sup}} \, \text{s}^{-1/2} \, \text{Einstein}^{-1/2}$	0.5×10^{11}	1.0×10^{11}
Ea^*	1.5×10^5	1.6×10^5	J mol^{-1}	2.9×10^4	2.4×10^4
$A_{H_2O}^*$	9.2×10^2	9.5×10^2	$\text{m}^3 \, \text{mol}^{-1}$	9.9×10^1	1.0×10^2
Ea_{H_2O}	1.4×10^4	1.5×10^4	J mol^{-1}	3.5×10^3	2.8×10^3
k'	4.0×10^3	5.3×10^3	$\text{m}^3_{\text{mix}} \, \text{m}^{-2}_{\text{sup}} \, \text{s}^{-1}$	1.1×10^2	6.4×10^2
Ea	0.9×10^5	0.9×10^5	J mol^{-1}	4.8×10^3	4.9×10^3
A_{H_2O}	10.0×10^2	9.9×10^2	$\text{m}^3 \, \text{mol}^{-1}$	2.1×10^2	1.5×10^2
Ea_{H_2O}	1.4×10^4	1.5×10^4	J mol^{-1}	3.3×10^3	3.7×10^3

Fig. 7. Ratio between CeTi and Ti kinetic parameters. Shaded area highlights the region of ratios equal to 1 within experimental error.

occurs under the primary use of light as energy source in the $k_{4.1}$ parameter. So, according to our kinetic analysis, the radical species interaction with the pollutant (a process triggered initially by light) is clearly favored in a thermo-photo process vs. the bare photo process (factors of 1.33 vs. 1.21).

In summary, using the above described kinetic formalism we detected rather similar absorption constants at the temperature range studied and considering the thermo-alone and the thermo-photo processes. This likely indicates that adsorption sites are differentiated from kinetically relevant actives sites and do not display important differences between the CeTi and Ti samples. This point also allows to analyze numerically the variation of the $k_{4.1}$ and $k_{4.2}$ kinetic constants and quantifying their enhancement in the composite system with respect to the parent titania reference (the reference dominating the molar composition of the material as well as the surface of the composite catalyst). The study shows that the ceria-titania interface displays enhanced activity with respect to its parent systems in both, thermo- and photo-parts of the process. The analysis allows uncoupling photo and thermo physical contributions but in fact shows that composite activity is defined by a "combined" thermo-photo effect. Scheme 1 attempts to provide a simplified representation of the main events taking place in the CeTi sample under the thermo-photo-oxidation of 2-propanol. The scheme displays that the interface between the oxide entities could be responsible (as previously discussed here and suggested in the literature for thermal and photo processes, see Refs. [11] and [49]) for thermo- and photo-related enhancement(s) of electron-related species and corresponding kinetic steps while a more efficient activation of the hole-related species could be associated to titania sites. The ceria-titania interface thus plays an important role in charge handling but also is an "active" center in the transformation of the pollutant. Such a hypothesis requires however further assessment. In any case, we would like to

performance in a pure thermo-based process to a larger degree than in the photo-catalytic process (1.32 vs. 1.21 factors). The larger enhancement is not a surprise considering that ceria is considered an excellent catalyst for VOC elimination [26–29]. However, our analysis provides a quantitative measurement of the differential performance and clearly indicates this to be a phenomenon related with the performance of the active centers involved (that is, the $k_{4.2}$ parameter). In this sense, we note that such centers are likely at the interface between the ceria and titania components and are unique for the composite catalysts in respect to the parent systems [49]. We also note that CeTi has increasing thermo-catalytic activity with respect to its parent Ce reference (Figs. 4 and 5). Equally interestingly, a larger enhancement

Scheme 1. Schematic view of the synergistic effect between photo- and thermo-catalysis on the CeTi sample.

highlight that the enhancement of activity has a main root in a more effective interaction of the oxidant species with the pollutant, achieved under both the thermal- and photo triggered steps of the mechanism and considering the joint use of both energy sources.

4. Conclusions

The catalytic performance of a ceria-titania composite system in the degradation of 2-propanol was analyzed with respect to the titania and ceria (parent) components using heat and light as energy sources of the reaction. The composite system displays an improved performance under the combined (as well as the independent) use of the two energy sources. This enhancement was analyzed using a kinetic formalism which explicitly includes the effect of the photon absorption in the reaction rate. The kinetic analysis is thus free of light-related, usual approximations (providing a scheme with potential general use) and expresses the rate as a sum of two components having different physico-chemical nature.

The fitting of the experimental data indicates that the high activity of the ceria-titania system is physically based in the cooperative use of light and heat energy sources. Quantitatively, we observed that the ceria-titania system has an enhancement factor a ca. 1.32 and 1.33 with respect to the parent systems in the kinetic constants controlling the active (oxygen and hydroxyl-type radical species, respectively) species responsible for the attack to the 2-propanol molecule in the degradation process. Such result indicates that the two energy sources work co-operatively, influencing each other in a bidirectional way, and rendering a true, heat-light synergistic interaction while using the composite system. The study thus shows that the ceria-titania works under a true thermo-photo-catalytic reaction scheme rather than a photo-assisted thermo or a thermo-assisted photo process. Such feature seems unique when compared with the titania and ceria reference systems, at least in the temperature region studied here for the 2-propanol degradation.

Appendix A. Supplementary data

Supplementary data associated with this article can be found, in the online version, at https://doi.org/10.1016/j.apcatb.2017.11.073.

References

[1] S. Wang, H.M. Ang, M.O. Tade, Environ. Int. 33 (2007) 694–705.
[2] A. Kubacka, M. Fernández-García, G. Colón, Chem. Rev. 112 (2012) 1555–1614.
[3] J.C. Colmenares, R. Luque, Chem. Soc. Rev. 43 (2014) 765–778.
[4] M.D. Hernández-Alonso, F. Fresno, S. Suárez, J.M. Coronado, Energy Environ. Sci. 2 (2009) 1231.
[5] O. Fontelles-Carceller, M.J. Muñoz-Batista, J.C. Conesa, M. Fernández-garcía, A. Kubacka, Appl. Catal. B Environ. 216 (2017) 133–145.
[6] C. Wang, J. Rabani, D.W. Bahnemann, J.K. Dohrmann, J. Photochem. Photobiol. A Chem. 148 (2002) 169–176.
[7] M.J. Muñoz-Batista, A. Kubacka, A.B. Hungría, M. Fernández-García, J. Catal. 330 (2015) 154–166.
[8] L. Satuf, R.J. Brandi, A.E. Cassano, O.M. Alfano, I. Universidad 46 (2007) 43–51.
[9] J. Cai, X. Wu, S. Li, F. Zheng, Appl. Catal. B Environ. 201 (2017) 12–21.
[10] Y. Wang, J. Zhao, T. Wang, Y. Li, X. Li, J. Yin, C. Wang, J. Catal. 337 (2016) 293–302.
[11] S. Luo, T.-D. Nguyen-Phan, A.C. Johnston-Peck, L. Barrio, S. Sallis, D.A. Arena, S. Kundu, W. Xu, L.F.J. Piper, E.A. Stach, D.E. Polyanskiy, E. Fujita, J.A. Rodriguez, S.D. Senanayake, J. Phys. Chem. C 119 (2015) 2669–2679.
[12] Z. Li, J. Sheng, Y. Zhang, X. Li, Y. Xu, Appl. Catal. B Environ. 166–167 (2015) 313–319.
[13] X. Sun, C. Li, L. Ruan, Z. Peng, J. Zhang, J. Zhao, Y. Li, J. Alloys Compd. 585 (2014) 800–804.
[14] C. Karunakaran, P. Gomathisankar, ACS Sustain. Chem. Eng. 1 (2013) 1555–1563.
[15] Y. Liu, P. Fang, Y. Cheng, Y. Gao, F. Chen, Z. Liu, Y. Dai, J. Chem. Eng. 219 (2013) 478–485.
[16] M. Zou, Y. Kong, J. Wang, Q. Wang, Z. Wang, B. Wang, P. Fan, Spectrochim. Acta. A Mol. Biomol. Spectrosc. 101 (2013) 82–90.
[17] Y. Wang, B. Li, C. Zhang, L. Cui, S. Kang, X. Li, L. Zhou, Appl. Catal. B Environ. 130–131 (2013) 277–284.
[18] H. Liu, M. Wang, Y. Wang, Y. Liang, W. Cao, Y. Su, J. Photochem. Photobiol. A Chem. 223 (2011) 157–164.
[19] C. Guzmán, G. del Ángel, R. Gómez, F. Galindo-Hernández, C. Ángeles-Chavez, Catal. Today 166 (2011) 146–151.
[20] V. Štengl, S. Bakardjieva, N. Murafa, Mater. Chem. Phys 114 (2009) 217–226.
[21] G. Li, D. Zhang, J.C. Yu, Phys. Chem. Chem. Phys. 11 (2009) 3775–3782.
[22] T. Tong, J. Zhang, B. Tian, F. Chen, D. He, M. Anpo, J. Colloid Interface Sci. 315 (2007) 382–388.
[23] S. Pavasupree, Y. Suzuki, S. Pivsa-Art, S. Yoshikawa, J. Solid State Chem. 178 (2005) 128–134.
[24] M.J. Muñoz-Batista, A. Kubacka, M.N. Gómez-Cerezo, D. Tudela, M. Fernández-García, Appl. Catal. B Environ. 140–141 (2013) 626–635.
[25] M.J. Muñoz-Batista, M. Ferrer, M. Fernández-García, A. Kubacka, Appl. Catal. B Environ. 154–155 (2014) 350–359.
[26] L.F. Liotta, M. Ousmane, G. Di Carlo, G. Pantaleo, G. Deganello, G. Marcì, L. Retailleau, A. Giroir-Fendler, Appl. Catal. A Gen. 347 (2008) 81–88.
[27] D. Delimaris, T. Ioannides, Appl. Catal. B Environ. 89 (2009) 295–302.
[28] D. Delimaris, T. Ioannides, Appl. Catal. B Environ. 84 (2008) 303–312.
[29] Q. Dai, X. Wang, G. Lu, Catal. Commun. 8 (2007) 1645–1649.
[30] M. Mao, H. Lv, Y. Li, Y. Yang, M. Zeng, N. Li, X. Zhao, ACS Catal. 6 (2016) 418–427.
[31] A.R. Almeida, R. Berger, J.A. Moulijn, G. Mul, Phys. Chem. Chem. Phys. 13 (2011) 1345–1355.
[32] L. Lan, Y. Li, M. Zeng, M. Mao, L. Ren, Y. Yang, H. Liu, L. Yun, X. Zhao, Appl. Catal. B Environ. 203 (2017) 494–504.
[33] M. Zeng, Y. Li, M. Mao, J. Bai, L. Ren, X. Zhao, ACS Catal. 5 (2015) 3278–3286.
[34] K. Huang, L. Lin, K. Yang, W. Dai, X. Chen, X. Fu, Appl. Catal. B Environ. 179 (2015) 395–406.
[35] H. Liu, Y. Li, Y. Yang, M. Mao, M. Zeng, L. Lan, L. Yun, X. Zhao, J. Mater. Chem. A 4 (2016) 9890–9899.
[36] F. Liu, M. Zeng, Y. Li, Y. Yang, M. Mao, X. Zhao, Adv. Funct. Mater. 26 (2016) 4518–4526.
[37] L. Ren, M. Mao, Y. Li, L. Lan, Z. Zhang, X. Zhao, Appl. Catal. B Environ. 198 (2016) 303–310.
[38] M. Zeng, Y. Li, F. Liu, Y. Yang, M. Mao, X. Zhao, Appl. Catal. B Environ. 200 (2017) 521–529.
[39] J. Gunschera, J.R. Andersen, N. Schulz, T. Salthammer, Chemosphere 75 (2009) 476–482.
[40] U.B. Celebi, N. Vardar, Atmos. Environ. 42 (2008) 5685–5695.
[41] D. Kotzias, Exp. Toxicol. Pathol. 57 (2005) 5–7.
[42] A.E. Cassano, C.A. Martin, R.J. Brandi, O.M. Alfano, Ind. Eng. Chem. Res. 34 (1995) 2155–2201.
[43] G.E. Imberdorf, H.A. Irazoqui, O.M. Alfano, A.E. Cassano, Chem. Eng. Sci. 62 (2007) 793–804.
[44] G.B. Raupp, A. Alexiadis, M.M. Hossain, R. Changrani, Catal. Today 69 (2001) 41–49.
[45] J. Klier, C.J. Tucker, T.H. Kalantar, D.P. Green, Adv. Mater. 12 (2000) 1751–1757.
[46] M. Fernández-García, X. Wang, C. Belver, J.C. Hanson, J.A. Rodriguez, J. Phys. Chem. C 111 (2007) 674–682.
[47] M.J. Muñoz-Batista, M.N. Gómez-Cerezo, A. Kubacka, D. Tudela, M. Fernández-García, ACS Catal. 4 (2014) 63–72.
[48] M.J. Muñoz-Batista, M. de los Milagros Ballari, A. Kubacka, A.E. Cassano, O.M. Alfano, M. Fernández-García, Chem. Eng. J. 255 (2014) 297–306.
[49] M.J. Muñoz-Batista, A. Kubacka, M. Fernández-García, ACS Catal. 4 (2014) 4277–4288.
[50] M.J. Muñoz-Batista, M.M. Ballari, A.E. Cassano, O.M. Alfano, A. Kubacka, M. Fernández-García, Catal. Sci. Technol. 5 (2014) 1521–1531.
[51] G.E. Imberdorf, A.E. Cassano, H.A. Irazoqui, O.M. Alfano, Chem. Eng. Sci. 62 (2007) 1138–1154.
[52] G.E. Imberdorf, A.E. Cassano, H.A. Irazoqui, O.M. Alfano, Catal. Today 129 (2007) 118–126.
[53] M.J. Muñoz-Batista, M.M. Ballari, A.E. Cassano, O.M. Alfano, A. Kubacka, M. Fernández-García, Catal. Sci. Technol. 5 (2015) 1521–1531.
[54] C. Passalía, M.E. Martínez Retamar, O.M. Alfano, R.J. Brandi, Int. J. Chem. React. Eng. 8 (2010).
[55] G.E. Imberdorf, H.A. Irazoqui, A.E. Cassano, O.M. Alfano, Ind. Eng. Chem. Res. 44 (2005) 6075–6085.
[56] G.L. Chiarello, D. Ferri, E. Selli, J. Catal. 280 (2011) 168–177.
[57] F. Arsac, D. Bianchi, J.M. Chovelon, A.C. Ferronato, J.M. Herrmann, J. Phys. Chem. A 110 (2006) 4202–4212.
[58] F. Arsac, D. Bianchi, J.M. Chovelon, C. Ferronato, J.M. Herrmann, J. Phys. Chem. A 110 (2006) 4213–4222.
[59] D. Brinkley, E. Thomas, J. Phys. Chem. B 102 (1998) 7596–7605.
[60] Y. Ohko, K. Hashimoto, A. Fujishima, J. Phys. Chem. A 101 (1997) 8057–8062.
[61] M.J. Muñoz-Batista, U. Caudillo-Flores, F. Ung-Medina, M. del Carmen Chávez-Parga, J.A. Cortés, A. Kubacka, M. Fernández-García, Appl. Catal. B Environ. 201 (2017) 400–410.